



# Composition of the Source Region Plasma in Inertial Electrostatic Confinement Devices

D.R. Boris and G.A. Emmert

August 2008

UWFDM-1344

To be published in *Physics of Plasmas*.

**FUSION TECHNOLOGY INSTITUTE**  
**UNIVERSITY OF WISCONSIN**  
**MADISON WISCONSIN**

### **DISCLAIMER**

This report was prepared as an account of work sponsored by an agency of the United States Government. Neither the United States Government, nor any agency thereof, nor any of their employees, makes any warranty, express or implied, or assumes any legal liability or responsibility for the accuracy, completeness, or usefulness of any information, apparatus, product, or process disclosed, or represents that its use would not infringe privately owned rights. Reference herein to any specific commercial product, process, or service by trade name, trademark, manufacturer, or otherwise, does not necessarily constitute or imply its endorsement, recommendation, or favoring by the United States Government or any agency thereof. The views and opinions of authors expressed herein do not necessarily state or reflect those of the United States Government or any agency thereof.

**Composition of the Source Region Plasma in  
Inertial Electrostatic Confinement Devices**

D.R. Boris and G.A. Emmert

Fusion Technology Institute  
University of Wisconsin  
1500 Engineering Drive  
Madison, WI 53706

<http://fti.neep.wisc.edu>

August 2008

UWFDM-1344

To be published in *Physics of Plasmas*.

## Abstract

The ion species composition in the source region of inertial electrostatic confinement (IEC) devices plays an important role in the atomic and molecular physics processes in the device and in the resulting energy spectrum of the fast ions and the neutron production rate. A zero dimensional rate equation model for the ion species composition in the source region of IEC devices is presented and compared with experimental measurements on the Wisconsin IEC device [J.F. Santarius, G.L. Kulcinski, *et al.*, Fusion Sci. Tech. **47**, 1238 (2005)]. The ion species composition is measured using an ion acoustic wave diagnostic; the results are in good agreement with the theoretical predictions. Both the theory and the experimental results show that  $D_3^+$  ions are the majority species in the source region.

## I. INTRODUCTION

The inertial electrostatic confinement (IEC) fusion concept was first patented by Farnsworth [1] in the 1960s and was advanced by Hirsch [2] shortly after Farnsworth's initial patent. The concept focuses on confining light ions using large negative electrostatic potentials in a spherically symmetric geometry. By placing a smaller, negatively biased, spherical cathode grid inside a grounded anode grid, ions produced outside the anode can be accelerated to fusion relevant energies. This confinement approach produces a non-Maxwellian plasma with increased ion density toward the center of the spherical geometry.

The IEC concept is of particular interest in the arena of non-electric applications of fusion, such as neutron sources for clandestine materials detection (explosives, chemical agents, fissile materials, etc.), and high energy proton sources for medical isotope production. The gridded IEC concept has been extensively investigated by research groups around the world. The University of Wisconsin [3], the University of Illinois Urbana-Champaign [4], and Los Alamos National Laboratory all have current research endeavors underway in the United States. This work has led to the first use of an IEC device to detect fissile material [5], and experimental verification of the periodically oscillating plasma sphere concept [6]. In addition, Kyoto University [7], Kansai University [8], and the Tokyo Institute of Technology [9] in Japan have research initiatives investigating the performance and applications of gridded IEC devices, including the first active testing of an IEC device as a means to detect anti-personnel land mines. The University of Sydney [10] in Australia has also made important diagnostic contributions to IEC research.

In typical IEC devices atomic and molecular processes play a significant role since the mean free path for ions to interact with the background gas is usually less than the size of the device. Molecular ions formed in the source region will undergo dissociative and charge exchange processes as they are being accelerated by the electric field between the two grids. This affects the energy spectrum and the resulting fusion reaction rate. In this paper the ion species mix in the ion source region, i.e. the region outside the anode, of IEC devices is investigated since it has an important role in determining the resulting atomic and molecular processes in the intergrid region, the energy spectrum of the ions at the center, and the resulting fusion reaction rate. A theoretical model of the ion mixture in the source region is described in Section II; experimental measurements of the ion mixture in the Wisconsin IEC device are reported in Section III.

## II. THEORETICAL MODEL OF THE SOURCE REGION

The source region (the region between the outer grid and the vacuum chamber walls) is modeled using zero dimensional rate equations to determine the composition of the ions crossing the outer grid (anode). The source region has a volume  $V$ , anode grid area  $A_g$ , wall area  $A_w$ , and is filled with deuterium gas. Electrons are emitted from filaments at an energy  $E_p$  (and speed  $v_p$ ). These electrons are referred to as primary electrons; they have a density  $n_p$ . Ionization processes produce colder electrons with density  $n_e$  and temperature  $T_e$ . Because of the strongly negative potential between the cathode and anode, electrons are confined to the source region and do not penetrate very far into the intergrid region. A sheath is set up at the anode grid that extracts ions from the source region plasma and accelerates them towards the cathode.

The primary electrons in the source region induce ionization and dissociation of the deuterium gas, ionization of the neutral deuterium atoms, and dissociation of the molecular ions. We assume the plasma in the source region is composed of  $D^+$ ,  $D_2^+$ , and  $D_3^+$  ions; impurity ions are neglected. We denote the density of the  $i$ th ion species as  $n_{i1}$  and the ion mass as  $m_i$ , where  $i=1$  denotes  $D^+$ ,  $i=2$  denotes  $D_2^+$ , and  $i=3$  denotes  $D_3^+$  ions. We also introduce the neutral atomic D species with density  $n_{10}$  and mass  $m_1$ , and neutral molecular  $D_2$  species with density  $n_{20}$  and mass  $m_2$ .

### A. Atomic and Molecular Interactions in the Source Region

To determine the species mix of the ions passing through the anode and entering the intergrid region, the atomic and molecular interactions shown in Table I are considered. Published cross-section, or reaction rate, data [11, 12, 13] is used. Note that most of the cross-section data available for these reactions are for normal hydrogen, not deuterium. The cross-sections should not be strongly isotope dependent, so we use hydrogen data where necessary for deuterium reactions. Another possible reaction is dissociative ionization of  $D_2^+$  ( $e + D_2^+ \rightarrow 2D^+ + 2e$ ); this competes with reaction (4) in Table I, but has a weaker cross-section [14, 15], so we neglect it.

Processes (2), (3), and (5) are driven by the energetic electrons from the filaments, so the relevant electron energy is the primary energy  $E_p$ . Processes (4), (6), and (8) are driven by the thermal electrons; the reaction rate is determined by integrating the cross-section over an

(assumed) Maxwellian distribution. We allow process (1) to be driven both by primary and thermal electrons. The interchange reaction, (7), has a large cross section at thermal energies [12].

## B. Rate Equations

We use zero-dimensional rate equations for the atom, molecular ion, and atomic ion densities. The neutral molecule density is assumed determined by the working gas pressure. We introduce  $c_i$  as the mean velocity at which ions of species  $i$  cross the presheath-sheath boundary at the anode grid and walls. The value of  $c_i$  is a subject of current research; we will choose two possibilities for  $c_i$  later.

The rate equation for the  $D_2^+$  ion density is

$$\frac{d}{dt}(n_{21}V) = n_p n_{20} \sigma_1 v_p V - \alpha_4 n_e n_{21} V - \alpha_1 n_e n_{21} V - \alpha_2 n_{21} n_{20} V - \frac{n_{21} c_2 (A_g + A_w)}{2}. \quad (1)$$

The first term on the right is the source due to ionization of the gas molecules, the second is the loss due to dissociation, the third is the loss due to dissociative recombination, the fourth is the

**Table I. Atomic and molecular processes considered.**

<b>Process</b>	<b>Interaction</b>	<b>cross section or reaction rate</b>
1. Ionization of $D_2$	$e + D_2 \rightarrow D_2^+ + 2e$	$\sigma_1$
2. Dissociation of $D_2$	$e + D_2 \rightarrow 2D + e$	$\sigma_2, \alpha_5$
3. Ionization of $D$	$e + D \rightarrow D^+ + 2e$	$\sigma_3$
4. Dissociation of $D_2^+$	$e + D_2^+ \rightarrow D^+ + D + e$	$\alpha_4$
5. Dissociative ionization of $D_2$	$e + D_2 \rightarrow D^+ + D + 2e$	$\sigma_5$
6. Dissociative recombination of $D_2^+$	$e + D_2^+ \rightarrow 2D$	$\alpha_1$
7. Interchange reactions producing $D_3^+$ ions	$D_2 + D_2^+ \rightarrow D_3^+ + D$	$\alpha_2$
8. Dissociative recombination of $D_3^+$ ions	$e + D_3^+ \rightarrow D_2 + D$	$\alpha_3$

loss due to interchange reactions, and the fifth is the flow to the walls and through the anode grid. The factor one-half arises because the density at the sheath edge is approximately one-half the density far from the sheath [16].

The rate equation for the neutral atom density is

$$\begin{aligned} \frac{d}{dt}(n_{10}V) = & 2(n_p\sigma_2v_p + n_e\alpha_5)n_{20}V + n_en_{21}\alpha_4V + 2\alpha_1n_en_{21}V + n_pn_{20}\sigma_5v_pV \\ & + \alpha_2n_{21}n_{20}V + \alpha_3n_en_{31}V - n_pn_{10}\sigma_3v_pV - n_{10}c_a(A_g + A_w) \end{aligned} \quad (2)$$

The first six terms on the right are the sources due to dissociation of gas molecules, dissociation of  $D_2^+$ , dissociative recombination of  $D_2^+$ , dissociative ionization of  $D_2$ , interchange reactions, and dissociative recombination of  $D_3^+$ , respectively. The seventh term is the loss due to ionization and the eighth term is the loss due to flow to the walls and through the anode grid. The variable  $c_a$  is the thermal velocity of the atoms,

$$c_a = \sqrt{\frac{kT_a}{m_a}} \quad (3)$$

The rate equation for the atomic ion density is

$$\frac{d}{dt}(n_{11}V) = n_pn_{10}\sigma_3v_pV + n_en_{21}\alpha_4V + n_pn_{20}\sigma_5v_pV - \frac{n_{11}c_1(A_g + A_w)}{2} \quad (4)$$

The three terms on the right are the sources due to ionization of neutral atoms, dissociation of  $D_2^+$ , and dissociative ionization of gas molecules, respectively. The fourth term is the flow to the walls and through the anode grid.

The rate equation for  $D_3^+$  ion density is

$$\frac{d}{dt}(n_{31}V) = \alpha_2n_{21}n_{20}V - \alpha_3n_en_{31}V - \frac{n_{31}c_3(A_g + A_w)}{2} \quad (5)$$

The first term on the right is the source due to interchange reactions, the second is the loss due to dissociative recombination and the third is the flow to the walls and through the anode grid.

Quasi-neutrality requires that

$$n_e + n_p = n_{21} + n_{11} + n_{31}. \quad (6)$$

We still need to determine the primary electron density. We do this indirectly by specifying the ion current passing through the anode grid,

$$I_{ion} = \frac{n_{11}c_1 + n_{21}c_2 + n_{31}c_3}{2} eA_g. \quad (7)$$

The set of equations, (1)-(7), are nonlinear so, before attempting to find the solutions, it is worthwhile to estimate the order of magnitude of the various terms and retain only the dominant terms. Using typical parameters for the University of Wisconsin Inertial Electrostatic (UW-IEC) device (2 mtorr D<sub>2</sub> gas,  $E_p = 200$  eV,  $I_{ion} = 15$  mA,  $V = 3.3 \times 10^5$  cm<sup>3</sup>,  $A_g = 7.8 \times 10^3$  cm<sup>2</sup>, and  $A_w = 1.7 \times 10^4$  cm<sup>2</sup>), we estimate the order of magnitude of the various source and loss terms in the rate equations. For the D<sub>2</sub><sup>+</sup> equation, Eq. (1), the important source term is ionization, and the important loss terms are interchange reactions and flow to the walls and anode; dissociation and dissociative recombination of D<sub>2</sub><sup>+</sup> are smaller by at least four orders of magnitude. For the D<sub>3</sub><sup>+</sup> equation, Eq. (5), the source is the interchange reaction; flow to the boundaries is the dominant loss, with dissociative recombination being about 3 to 4 orders of magnitude weaker. For the neutral atom rate equation, Eq. (2), interchange reactions and dissociation of D<sub>2</sub> are the dominant sources. Flow to the boundaries is the dominant loss term; ionization of D is weaker by about six orders of magnitude. For the D<sup>+</sup> equation, Eq. (4), dissociative ionization of D<sub>2</sub> is the dominant source term and flow to the boundaries is the only loss term. These results arise partly because of the magnitudes of the relevant cross sections, but also because the background gas density,  $n_{20}$ , is the dominant density in our IEC device; all other densities are smaller by at least four orders of magnitude.

A consequence of dissociative ionization of D<sub>2</sub> dominating over simple ionization of D is that the rate equations for the ion densities (D<sup>+</sup>, D<sub>2</sub><sup>+</sup>, D<sub>3</sub><sup>+</sup>) become decoupled from the rate equation for the neutral atom density. This simplifies the analysis.

Assuming steady-state and retaining only the dominant source and loss terms, the rate equations become

$$D^+ \text{ ions: } n_p n_{20} \sigma_5 v_p V - 0.5 n_{11} c_1 (A_g + A_w) = 0 \quad (8)$$

$$D_2^+ \text{ ions: } n_p n_{20} \sigma_1 v_p V - \alpha_2 n_{21} n_{20} V - 0.5 n_{21} c_2 (A_g + A_w) = 0 \quad (9)$$

$$D_3^+ \text{ ions: } \alpha_2 n_{21} n_{20} V - 0.5 n_{31} c_3 (A_g + A_w) = 0 \quad (10)$$

$$\text{Ion current: } n_{11} c_1 + n_{21} c_2 + n_{31} c_3 = \frac{2I_{ion}}{eA_g} . \quad (11)$$

At this point we need to specify the flow velocities  $c_1$ ,  $c_2$ , and  $c_3$ . For a truly collisionless plasma these should be independent; one possibility is to take each at their individual Bohm velocity,

$$c_i = \sqrt{\frac{kT_e}{m_i}} . \quad (12)$$

However, recent experimental and theoretical work by Hershkowitz and co-workers [17, 18] for a mildly collisional plasma leads to each species entering the sheath at the same velocity, namely a concentration-weighted drift velocity that satisfies the Bohm criteria,

$$c_1 = c_2 = c_3 = \sqrt{\frac{kT_e}{n_e} \left( \frac{n_{11}}{m_1} + \frac{n_{21}}{m_2} + \frac{n_{31}}{m_3} \right)} . \quad (13)$$

We begin with the first choice, Eq. (12), and then consider the differences caused by the second choice, Eq. (13).

Using Eq. (12) for  $c_i$ , the set of equations (8) – (11) are linear and can be written in matrix form

$$\begin{pmatrix} n_{20} \sigma_5 v_p V & -0.5 c_1 (A_g + A_w) & 0 & 0 \\ n_{20} \sigma_1 v_p V & 0 & -\alpha_2 n_{20} V - 0.5 c_2 (A_g + A_w) & 0 \\ 0 & 0 & \alpha_2 n_{20} V & -0.5 c_3 (A_g + A_w) \\ 0 & c_1 & c_2 & c_3 \end{pmatrix} \begin{pmatrix} n_p \\ n_{11} \\ n_{21} \\ n_{31} \end{pmatrix} = \begin{pmatrix} 0 \\ 0 \\ 0 \\ \frac{2I_{ion}}{eA_g} \end{pmatrix} \quad (14)$$

Inverting the coefficient matrix gives the solution for the various densities.

For the second choice for  $c_i$  (Eq. (13)), the set of equations (8)-(11) are no longer linear since the  $c_i$  contain the various densities. To solve this, we use an iterative technique using the densities obtained from the solution to Eq. (14) as a starting point; using these densities,  $c_i$  is recalculated from Eq. (13), which then allows the matrix inversion to give a new set of densities. This iterative process is continued until convergence is achieved, which is typically in 3 to 4 iterations.

Once the ion densities are determined, we then determine the neutral atom density from Eq. (2):

$$n_{10} = \frac{2(n_p \sigma_2 v_p + n_e \alpha_5) n_{20} V + n_e n_{21} (\alpha_4 + 2\alpha_1) V + n_p n_{20} \sigma_5 v_p V + \alpha_2 n_{21} n_{20} V + \alpha_3 n_e n_{21} V}{n_p \sigma_3 v_p V + c_a (A_g + A_w)}. \quad (15)$$

### C. Preliminary Results

To get a preliminary estimate of the ion mix in the source region we use nominal values for the Wisconsin IEC device [3] (background gas is  $D_2$  at 2 mtorr, anode ion current of 15 mA, 200 eV primary electron energy, 2 eV thermal electron temperature,  $V = 2.66 \times 10^6 \text{ cm}^3$ ,  $A_g = 7.85 \times 10^3 \text{ cm}^2$ ,  $A_w = 1.70 \times 10^4 \text{ cm}^2$ ). Using the assumption that each species enters the sheath at their own Bohm velocity, the resulting ion mix is 74%  $D_3^+$ , 22%  $D_2^+$ , 4%  $D^+$  for the ion density in the source region, and 69%  $D_3^+$ , 25%  $D_2^+$ , 6%  $D^+$  for the ion current extracted through the anode grid. If, instead, we assume that the different ion species enter the sheath with the same drift velocity, then the resulting ion mix is 71%  $D_3^+$ , 23%  $D_2^+$ , 6%  $D^+$  for both the ion density and the extracted ion current. The choice for the assumption concerning the ion drift velocity at the sheath edge does not greatly affect the results; the  $D_3^+$  ions dominate the ion mixture in the source region with both assumptions. Varying the parameters over reasonable ranges did not seem to make much difference to the basic conclusion that  $D_3^+$  dominates the ion mix. This is primarily because of the large cross section for the interchange reaction.

### D. Modification when cathode is at ground potential

The above analysis assumes the cathode is at a large negative potential so the source region is confined to the region outside the anode grid. In the experimental measurements reported in Sect. III, the cathode is at ground potential; this requires a minor modification to the theory. In this case the source region becomes the entire chamber volume, and flow through the anode grid is no longer a loss term. In addition, the extracted ion current to the cathode is no longer relevant,

so instead we use the measured ion saturation current on a Langmuir probe in the source region to close the set of equations. With these changes, the set of equations to be solved become

$$\begin{pmatrix} n_{20}\sigma_5v_pV & -0.5c_1A_w & 0 & 0 \\ n_{20}\sigma_1v_pV & 0 & -\alpha_2n_{20}V - 0.5c_2A_w & 0 \\ 0 & 0 & \alpha_2n_{20}V & -0.5c_3A_w \\ 0 & c_1 & c_2 & c_3 \end{pmatrix} \begin{pmatrix} n_p \\ n_{11} \\ n_{21} \\ n_{31} \end{pmatrix} = \begin{pmatrix} 0 \\ 0 \\ 0 \\ \frac{2I_{ionp}}{eA_p} \end{pmatrix} \quad (16)$$

which is solved either directly, or iteratively, depending on the choice for  $c_i$ , in the same manner as in subsection B above. In Eq. (16),  $I_{ionp}$  is the ion saturation current to the probe, and  $A_p$  is the probe collection area. Numerical solutions when the cathode is not at a high negative voltage, i.e. solving Eq. (16), are qualitatively similar to those when the cathode is at a high negative voltage, i.e. solving Eq. (14); in both situations  $D_3^+$  is the dominant ion species.

### III. EXPERIMENTAL MEASUREMENT OF THE ION MIXTURE IN THE SOURCE REGION

#### A. Multispecies Ion Acoustic Wave Dispersion Relation

In order to experimentally measure the ion mixture in the source region, a method to measure the concentration-weighted reduced ion mass of the source plasma was devised by utilizing the characteristics of multi-species ion acoustic waves. Since the source region of the UW-IEC device consists of a filament-assisted dc discharge, the source plasma can be treated as a cold, non-magnetized plasma. By measuring the phase velocity of ion acoustic waves propagated in the source region, a concentration-weighted reduced ion mass can be obtained for the plasma, provided that the electron temperature is known.

For a general electrostatic wave in a collisionless, non-drifting plasma of  $n$  ion species, the dispersion relation is given by

$$1 = \frac{\omega_{pe}^2}{\omega^2 - (kv_{th,e})^2} + \sum_{j=1}^n \frac{\omega_{pj}^2}{\omega^2 - (kv_{th,j})^2} \quad (17)$$

where the plasma frequency and thermal velocity of the  $j$ th ion species in the plasma is represented by  $\omega_{pj}$  and  $v_{thj}$ , respectively, and  $\omega_{pe}$  and  $v_{the}$  represents the plasma frequency and thermal velocity of the electrons, respectively. The primary electrons produced by emission from the filaments have a much lower density than the thermal electrons, so we neglect them in the dispersion relation. If cold ions are assumed then the dispersion relation simplifies to

$$1 = \frac{\omega_{pe}^2}{\omega^2 - (kv_{the})^2} + \sum_{j=1}^n \frac{\omega_{pj}^2}{\omega^2}. \quad (18)$$

For ion electrostatic waves such as those considered here, the phase velocity of the wave,  $\omega/k$ , will be significantly lower than the electron thermal velocity,  $v_{the} = \sqrt{2kT_e/m_e}$ ; this allows Eq. (18) to be simplified to

$$1 = -\frac{\omega_{pe}^2}{(kv_{the})^2} + \sum_{j=1}^n \frac{\omega_{pj}^2}{\omega^2} \quad (18a)$$

which can be re-expressed as

$$1 + \frac{1}{(\lambda_D k)^2} = \sum_{j=1}^n \frac{\omega_{pj}^2}{\omega^2}. \quad (19)$$

Since the plasmas dealt with in the context of the IEC source region are filament-assisted dc discharge plasmas, where the Debye length,  $\lambda_D = \sqrt{\epsilon_0 kT_e / ne^2}$ , is on the order of 1 mm, and the  $k$  of the propagated wave was typically  $100 \text{ m}^{-1}$ , the ratio quantity  $(\lambda_D k)^{-2} \gg 1$  [19]. Thus we can re-express Eq. (19) as follows,

$$\frac{1}{(\lambda_D k)^2} \approx \sum_{j=1}^n \frac{\omega_{pj}^2}{\omega^2}. \quad (19a)$$

This leads to the following real solution for the dispersion relation

$$\frac{\omega}{k} = \sqrt{\sum_{j=1}^n c_{sj}^2}. \quad (20)$$

In this expression the terms  $c_{sj} = \sqrt{n_j k T_e / n_e m_j}$  are the concentration-weighted ion acoustic velocities of the individual plasma species. The dispersion relation can be re-expressed in terms of the square of the phase velocity  $v_{ph}$ ,

$$v_{ph}^2 = \sum_{j=1}^n \frac{n_j k T}{n_e m_j} . \quad (21)$$

Consequently, a concentration-weighted reduced ion mass can be obtained from the phase velocity of the ion acoustic waves,

$$M_R = \frac{1}{\sum_{j=1}^n \frac{n_j}{n_e m_j}} = \frac{k T_e}{v_{ph}^2} . \quad (22)$$

## B. Experimental Method

Measurements of the concentration weighted reduced ion mass of a deuterium plasma were undertaken in the University of Wisconsin IEC experiment [3]. The UW-IEC experiment is a fusion device that operates by confining ions in a deep electrostatic potential well, in which the ions are accelerated to fusion relevant energies. The vacuum vessel of the UW-IEC experiment consists of a large cylindrical aluminum chamber 91 cm in diameter and 66 cm in height. A turbo pump provides a nominal base pressure of between  $1 \times 10^{-6}$  and  $5 \times 10^{-6}$  torr. Within the vacuum chamber are two concentric spherical metal grids used to create the potential well discussed above. The outer grid serves as an anode and is held at ground potential, while the inner grid is connected to a high (negative) voltage power supply. The inner grid is connected to the power supply through an insulated high voltage feedthrough, and acts as the cathode of the system. Typical voltages on the inner grid are between -100 kV and -150 kV. The source of the fuel ions for this experiment is a cold, low density ( $10^7$  to  $10^8$  cm<sup>-3</sup>), weakly ionized, filament-assisted dc discharge plasma that exists between the wall of the vacuum vessel and anode of the device. The measurements of the concentration-weighted reduced ion mass were performed in this source region. The high voltage system was not in operation during these experiments. In addition to the safety concerns inherent to using Langmuir probes in close proximity to high voltage electrodes, the high voltage cathode was not used because the potential from the cathode creates islands of negative potential within the holes in the anode grid. These potential islands

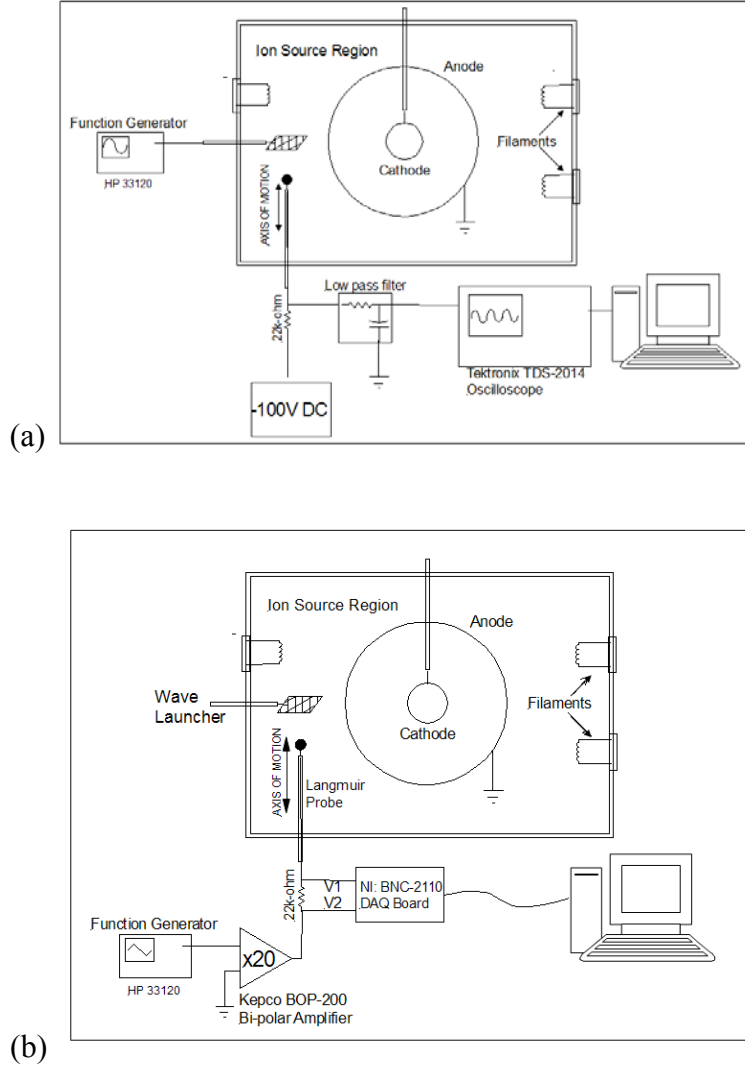


FIG. 1. The above figure shows the experimental setup for **(a)** the measure of the received ion acoustic wave signal as a function of distance from the continuous wave source, and **(b)** the setup for measuring the electron temperature as a function of distance from the wave source.

would substantially complicate the interpretation of ion acoustic wave data taken in the source region by locally perturbing the plasma potential in the affected regions. In addition the cathode pulls ions from the source region reducing the density in the source region ( to  $\sim 10^6 \text{ cm}^{-3}$ ) to the point where the signal to noise ratio for the detected ion acoustic waves becomes a concern.

The method used for obtaining a measurement of the concentration-weighted reduced ion mass is detailed below. A Langmuir probe, moveable along a designated axis, can be used to sample the

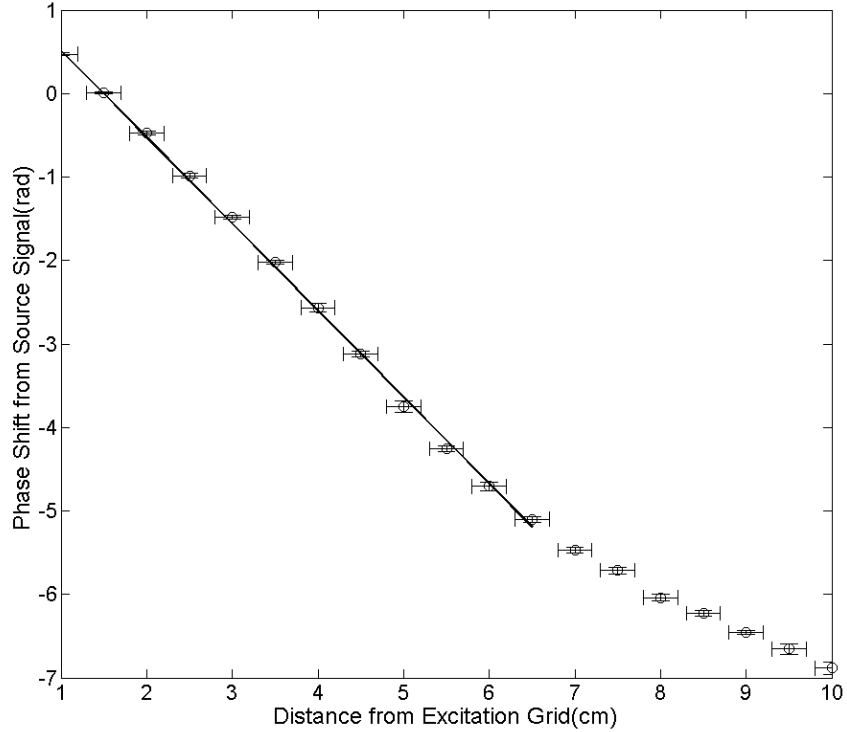


FIG. 2. The above data corresponds to the phase shift of a 100 kHz wave moving through a plasma with a nominal electron temperature of 2.7 eV. This leads to a calculated weighted reduced ion mass of 5.9 amu  $\pm$  0.5 amu. The neutral gas pressure for this data set was 3.0 mtorr.

ion acoustic wave at varying distances from the excitation source, as shown in Fig. 1a. The excitation source utilizes a continuous sine wave signal which is propagated through the plasma by a 75 cm<sup>2</sup> wave launcher made of a stainless steel mesh. Since the excitation signal is a continuous wave, the received signal on the Langmuir probe will have a quantifiable phase shift from the source signal at varying distances from the wave launcher. This was done by holding the probe at a constant bias of -100 V and sampling the wave along the axis, as shown in Fig. 1a. By measuring the rate at which this phase shift changes with increasing distance from the excitation source, the wave number,  $k$ , of the ion acoustic wave can be directly measured [20]. The oscilloscope used to analyze the received signal also provides the frequency of the ion acoustic wave, thus the phase velocity is easily calculated. The phase shift of the received signal from the excitation signal, for varying distances from the wave launcher, is plotted in Fig. 2.

In addition to sampling the ion acoustic wave signal, the Langmuir probe was also used to measure the electron temperature at varying distances from the excitation source. The experimental setup for measuring the electron temperature is shown in Figure 1b.

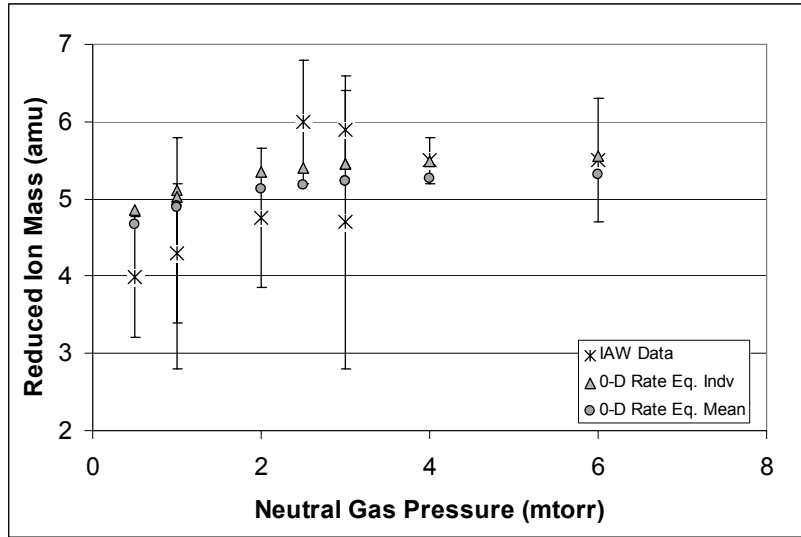
In order to reduce noise on the received signal the received waveform is first sent through a low pass RC filter. In addition to the low pass filter, a 128 trace average of the received signal is taken using a Tektronix TDS-2014 oscilloscope. This serves to further reduce high frequency components in the signal. With a direct measurement of the phase velocity of the ion acoustic wave the concentration-weighted reduced ion mass can easily be obtained.

### C. Experimental Results and Comparison to Theory

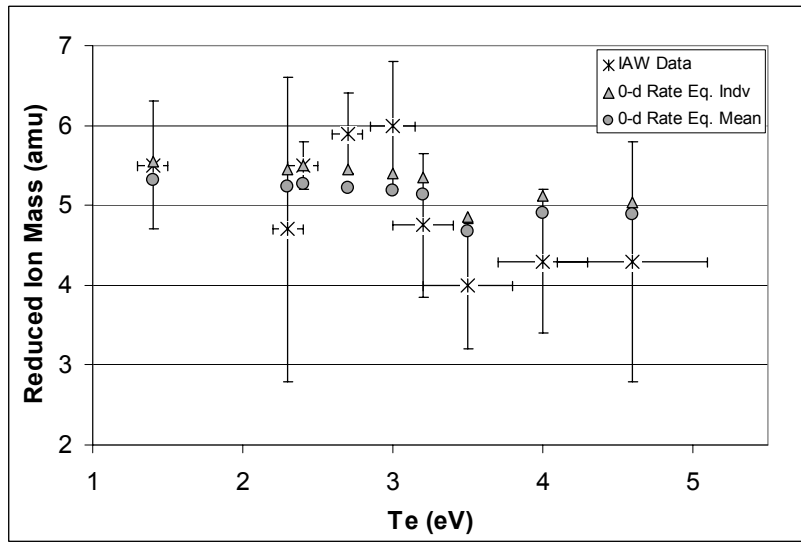
From the phase velocity of the wave and measured electron temperature in the IEC source region a concentration-weighted reduced ion mass can be calculated using Eq. (22). Figure 3 shows the variation of  $M_R$  with neutral gas pressure and electron temperature. The measured values are compared with the  $M_R$  values predicted from the ion concentrations calculated by the rate equation model described in Section II. The comparison is generated by using the measured parameters of filament bias, electron temperature, and neutral gas pressure from the experimental data points as inputs into the rate equation calculation. Two versions of the rate equation calculation were executed; the first version assumed molecular ion flow out of the source plasma at the ion sound speed of the individual ion species. The second version assumed ion flow out of the source plasma at the concentration-weighted mean ion acoustic velocity, as indicated in the work by Hershkowitz and co-workers [17, 18]. In both cases the calculated ion species concentrations were used to determine the concentration-weighted reduced ion mass for comparison to the measured values. The error in the measured values is due primarily to the error in the  $v_{ph}$  measurement in conjunction with the error in the measurement of  $kT_e$ .

In general the agreement between the rate equation analysis and experiment was quite good at lower electron temperatures and high neutral gas pressures. The calculated values fell within the error of the experiment for all measurements and the calculated molecular ion concentrations were generally able to reproduce the trends observed in the experimental data. In general the  $M_R$  of the source plasma was larger (nearer to 6 amu) at low electron temperature and high neutral gas pressure, and smaller (nearer to 4 amu) at high electron temperature and low neutral gas

pressure. It is reasonable to infer that the higher  $M_R$  values correspond with conditions where the interchange reaction between  $D_2^+$  ions and  $D_2$  neutrals dominate. Such conditions are conducive to high concentrations of  $D_3^+$  ions. Conversely the lower  $M_R$  values correspond to conditions where more evenly distributed mixtures of  $D_3^+$ ,  $D_2^+$ , and  $D^+$  ions are present. Khachan and Collis[10] have measured  $H_2^+$  and  $H_3^+$  in an IEC device operating on hydrogen; their measurements yielded a mixture of 20%  $H_3^+$  in the cathode region. We expect that the fraction of  $H_3^+$  in the cathode region will be significantly reduced from that in the source region by charge exchange and dissociative processes with the background neutral gas that occur between the source region and the cathode region. We point this out in order to avoid confusion, as the measurements performed by Khachan and Collis deal with a fundamentally different region of an IEC device.



(a)



(b)

FIG. 3. Comparison of experimental and theoretical concentration-weighted reduced ion mass. **(a)** At low neutral gas pressure the ion species mix contains a significant fraction of  $D_2^+$ , whereas at high neutral gas pressure  $D_3^+$  is the dominant ion type. **(b)** Low electron temperature plasmas contain mostly  $D_3^+$ ; the fraction of  $D_3^+$  is reduced as the electron temperature increases.

## IV. CONCLUSIONS

Rate equations have been used to determine the ion species mix in the source region of IEC devices. The results show that the dominant ion species is  $D_3^+$ , with  $D_2^+$  and  $D^+$  present in lesser amounts. Experimental measurements of the concentration-weighted reduced ion mass in the UW-IEC device are reasonably consistent with that calculated from the ion species mix obtained from the rate equation analysis. Measurements of the source region with the cathode in operation indicate similar source plasma parameters to those measured in this experiment, except for a reduced plasma density. In addition, the rate equation model indicates that these source plasma conditions produce similar molecular ion concentrations to those measured in this experiment. Thus we find the rate equation model to be a good predictor of the source plasma conditions during normal high voltage operation of the UW-IEC device. Quantitative knowledge of the species composition of the ions leaving the source region and entering the intergrid region is important for understanding the molecular processes occurring in the intergrid region, the composition and energy spectrum of the fast ions near the cathode, the generation of fast neutral atoms and molecules by charge exchange processes, and the resulting fusion reaction rate. Changes to the source region that modify the ion species composition offer the possibility of improving the performance of IEC devices.

## ACKNOWLEDGEMENTS

We gratefully acknowledge helpful discussions with Dr. John Santarius and Dr. Noah Hershkowitz. Research supported by U.S. Dept. of Energy grant DE-FG02-04ER54745 and by the Grainger Foundation.

## REFERENCES

- <sup>1</sup> P.T. Farnsworth, “*Electric Discharge Device for Producing Interaction Between Nuclei*”, U.S. Patent #3,258,402, patented June 28, 1966.
- <sup>2</sup> R.L. Hirsch, J. Appl. Phys. **38** (1967) 4522.
- <sup>3</sup> J.F. Santarius, G.L. Kulcinski, *et al.*, Fusion Science Tech. **47**, 1238 (2005).
- <sup>4</sup> G. H. Miley, J. Sved, Appl. Radiat. Isot. **48**, 1557 (1997).

- <sup>5</sup> R.F. Radel, G.L. Kulcinski, *et al.*, Fusion Sci. Tech. **52**, 1087 (2007).
- <sup>6</sup> J. Park, R.A. Nebel, S. Stange, and S. Krupakar Murali, Phys. Rev. Lett. **95**, 015003 (2005).
- <sup>7</sup> K. Yoshikawa, K. Masuda, Teruhisa Takamatsu, Seiji Shiroya, Tsuyoshi Misawa, Eiki Hotta, Masami Ohnishi, Kunihito Yamauchi, Hodaka Osawa and Yoshiyuki Takahashi, Nucl. Instr. Meth. Phys. Res. B **261**, 299 (2007).
- <sup>8</sup> H. Osawa, T. Kawame, S. Yoshioku, M. Ohnishi, 20th IEEE/NPSS Sym. Fusion Eng., SOFE **03**, 316 (2003).
- <sup>9</sup> K. Yamauchi, Masato Watanabe, Akitoshi Okino, Toshiyuki Kohno, Eiki Hotta, Morimasa Yuura, Fusion Sci. Tech. **47**, 1229 (2005).
- <sup>10</sup> J. Khachan and S. Collis, Phys. Plasmas, **8**, 1299 (2001).
- <sup>11</sup> See National Technical Information Service Document No. ORNL-5207 (C. F. Barnett, “*Atomic Data for Controlled Fusion*”, ORNL Report 5207, vol. II 1977), pg. C.3.2, C.4.2, C.4.8, C.4.10, C.4.34, C.7.2, C.7.6. Copies may be ordered from the National Technical Information Service, Springfield VA 22161.
- <sup>12</sup> See National Technical Information Service Document No. DE91000527 (H.T. Hunter, M.I. Kirkpatrick, I. Alvarez, C. Cisneros, and R.A. Phaneuf, “*Collisions of H, H<sub>2</sub>, He, and Li atoms and ions with atoms and molecules*”, ORNL Report 6086, vol. I, July 1990), pg. H-10. Copies may be ordered from the National Technical Information Service, Springfield VA 22161.
- <sup>13</sup> B. Peart and K.T. Dolder, J. Phys. B: Atom., Molec. Phys. **7**, 1948 (1974).
- <sup>14</sup> G.H. Dunn and B. Van Zyl, Phys. Rev. **154**, 40 (1967).
- <sup>15</sup> H. Takawara, Y. Itakawa, H. Nishimura, and M. Yoshino, J. Phys. Chem. Ref. Data **19**, 617 (1990).
- <sup>16</sup> N. Hershkowitz, Phys. Plasmas **12**, 055502 (2005).
- <sup>17</sup> D. Lee, N. Hershkowitz, and G. Severn, Appl. Phys. Lett. **91**, 041505 (2007).
- <sup>18</sup> D. Lee, L. Oksuz, and N. Hershkowitz, Phys. Rev. Lett. **99**, 155004 (2007).
- <sup>19</sup> A.M. Hala and N. Hershkowitz, Rev. Sci. Instr. **72**, 5, 2279 (2001).
- <sup>20</sup> X. Wang and N. Hershkowitz, Phys. Plasmas **13**, 053503 (2006).